Journal of Electronics, Electromedical Engineering, and Medical Informatics
Homepage: jeeemi.org; Vol. 7, No. 4, October 2025, pp: 1045-1059 e ISSN: 2656 8632

RESEARCH ARTICLE OPEN ACCESS

H20 and H20 with NaOH-Based Multispectral Classification Using Image Segmentation and Ensemble Learning EfficientNetV2, Resnet50, MobileNetV3

Melinda Melinda[1], Yunidar Yunidar[1], Zulhelmi Zulhelmi[1], Arya Suyanda[1], Lailatul Qadri Zakaria[2], and W.K Wong[3]

[1] Department of Electrical and Computer Engineering, Universitas Syiah Kuala, Banda Aceh, Indonesia
[2] Faculty of Information Science and Technology, Universiti Kebangsaan Malaysia, Bangi, Selangor, Malaysia
[3] Department of Electrical and Computer Engineering, Faculty of Engineering and Sciences. Curtin University Malaysia, Sarawak, Malaysia

Corresponding author: Melinda Melinda. (e mail: melinda@usk.ac.id), **Author(s) Email**: Yunidar Yunidar (e mail: yunidar@usk.ac.id), Zulhelmi Zulhelmi (e mail: zulhelmi@usk.ac.id), Arya Suyanda (e mail: arya.su@mhs.usk.ac.id), Lailatul Qadri Zakaria (e mail: lailatul.qadri@ukm.edu.my), W.K Wong (e mail: WeiKitt.w@curtin.edu.my)

Abstract **High Multispectral imaging has become a promising approach in liquid classification, particularly in distinguishing visually similar but subtly spectrally distinct solutions, such as pure water (H_2O) and water mixed with sodium hydroxide (H_2O with NaOH). This study proposed a classification system based on image segmentation and deep learning, utilizing three leading Convolutional Neural Network (CNN) architectures: ResNet 50, EfficientNetV2, and MobileNetV3. Before classification, each multispectral image was processed through color segmentation in HSV space to highlight the dominant spectral, especially in the hue range of 110 170. The model was trained using a data augmentation scheme and optimized with the Adam algorithm, a batch size of 32, and a sigmoid activation function. The dataset consists of 807 images, including 295 H_2O images and 512 H_2O with NaOH images, which were divided into training (64%), validation (16%), and testing (20%) data. Experimental results show that ResNet50 achieves the highest performance, with an accuracy of 93.83% and an F1 score of 93.67%, particularly in identifying alkaline pollution. EfficientNetV2 achieved the lowest loss (0.2001) and exhibited balanced performance across classes, while MobileNetV3, despite being a lightweight model, remained competitive with a recall of 0.97 in the H_2O with NaOH class. Further evaluation with Grad CAM reveals that all models focus on the most critical spectral areas of the segmentation results. These findings support the effectiveness of combining color-based segmentation and CNN in the spectral classification of liquids. This research is expected to serve as a stepping stone in the development of an efficient and accurate automatic liquid classification system for both laboratory and industrial applications.**

Keywords **Multispectral Classification, CNN, ResNet50, EfficientNetV2, MobileNetV3, HSV Segmentation, Liquid Spectral Image.**

I. Introduction

Progress in image-based material classification, especially for objects that are difficult to distinguish visually. One approach that is now receiving widespread attention is multispectral imaging, an image acquisition technique that captures the spectral information of an object as a whole by utilizing different wavelengths [13], [18], [31]. This technology has been widely applied in agriculture, medicine, geology, and the chemical industry, with the main advantage of detecting spectral variations that cannot be identified by the human eye [1], [3], [7]. One of the most significant challenges in this domain is the classification of aqueous fluids, such as pure water (H_2O) and H_2O with a NaOH solution, as they exhibit very subtle spectral differences and often overlap in visual representation. These spectral differences often manifest as subtle intensity shifts in the near-infrared region, which are difficult to capture using conventional RGB imaging alone. Multispectral imaging addresses this challenge by enabling the acquisition of wavelength-specific reflectance data, thereby

Manuscript received June 8, 2025; Revised August 20, 2025; Accepted September 5, 2025; date of publication September 10, 2025
Digital Object Identifier (**DOI**): https://doi.org/10.35882/jeeemi.v7i4.1016

enhancing the detection of solute-induced spectral deviations that are otherwise invisible to the human eye. Electrical impedance and solution conductivity-based approaches have been used to distinguish these chemical characteristics [19], [25]. However, these methods have limitations, as they are contact-based, time-consuming, and cannot be applied in real-time in image-based automated systems [6], [7]. Several previous studies have advocated the use of High Fluctuation (HF)-based spectral segmentation in HSV color space to extract dominant information from liquid images. This segmentation has been shown to improve the representation of spectral patterns between H_2O and H_2O with NaOH and has been used in several previous publications [21], [22].

Furthermore, a radiation-based spectral subtraction method was also introduced to improve the signal-to-noise ratio (SNR) and the accuracy of visual intensity readings from solution spectra [23]. For instance, both solutions reflect similarly across visible bands (400–700 nm), while subtle spectral shifts can appear in the near-infrared region (700–900 nm), influenced by NaOH solubility effects [34]. Multispectral imaging enables the detection of such nuanced variations. In addition, several techniques such as spectroscopy-based classifiers, Support Vector Machines (SVM), and traditional image thresholding have been explored. However, these methods often suffer from limited robustness when dealing with high spectral overlap, especially in fluid-based chemical mixtures where visual and spectral differences are minimal [32], [33]. For example, SVM classifiers rely heavily on handcrafted features, which may not capture subtle spectral shifts, while thresholding methods lack the adaptability needed for complex multispectral variations. This limitation highlights the necessity of deep learning-based approaches capable of learning abstract spectral representations from raw or minimally processed images. In the context of automatic classification, Convolutional Neural Networks (CNN) have become the de facto standard due to their ability to recognize complex visual patterns. Some common CNN architectures used include ResNet50, which excels in extracting deep features with training stability thanks to residual learning [11]; EfficientNetV2, designed for fast training and high parameter efficiency [3]; and MobileNetV3, which is aimed at resource-constrained devices yet remains competitive in accuracy [16] . These architectures were chosen over alternatives like DenseNet or Inception due to their balance of depth, speed, and proven performance in similar multispectral and hyperspectral classification tasks [35] .

Although each architecture has its advantages, a single approach is often less stable when applied to very similar spectral data. Therefore, this study proposes an ensemble system that combines the three architectures with HF segmentation-based preprocessing and a reliable method for classifying chemical solutions with minimal visual differences.

The integration of three CNN architectures, ResNet50, EfficientNetV2, and MobileNetV3, into a single HF segmentation image-based ensemble system, aims to improve the stability, efficiency, and accuracy of H_2O and H_2O with NaOH solution image

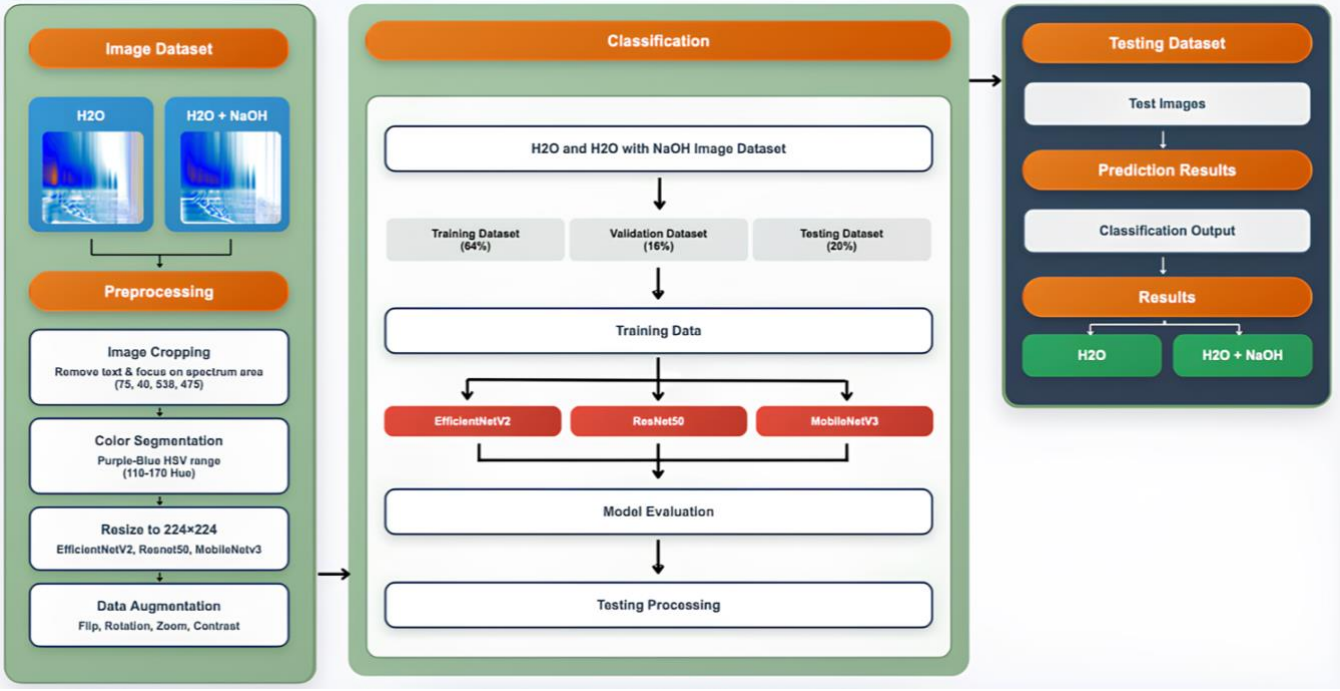

Fig. 1. Research flow in H2O and H2O with NaOH image

Manuscript received June 8, 2025; Revised August 20, 2025; Accepted September 5, 2025; date of publication September 10, 2025
Digital Object Identifier (**DOI**): https://doi.org/10.35882/jeeemi.v7i4.1016

classification. This study also employed preprocessing techniques, including active spectral cropping, HSV color segmentation, and data augmentation, to enhance the diversity of visual features.

The main contributions of this research are as follows:

1. Proposing the integration of a CNN ensemble system (ResNet50, EfficientNetV2, and Mo bileNetV3) for the classification of H_2O and H_2O solutions with NaOH based on multispectral images, which has not been studied thoroughly in previous literature.
2. Applying High Fluctuation (HF) based spectral segmentation in the HSV color space to extract the most informative dominant spectral areas, thereby improving the visual representation before classification.
3. Converted .dat experimental data into two-dimensional spectral images using MATLAB, with custom color mapping and logarithmic transformation to optimize the spectral representation.
4. Evaluating the effectiveness of CNN preprocessing, augmentation, and ensemble strategies in improving the classification accuracy of chemical solutions with very subtle spectral differences.
5. Providing an adaptable approach for multispectral camera-based real-time classification systems in the fluid chemical industry or other non-contact spectral detection systems.

All stages of the research, from converting .dat data into spectral images and preprocessing to bluish-purple-based segmentation, classification, and evaluation of the CNN model, are systematically explained in the research flow, as illustrated in Fig. 1.

II. Materials and Methods

This study utilized spectral signal data derived from high-frequency measurements of pure H_2O and H_2O mixed with NaOH. The data was collected using a MATLAB-based acquisition system and originated from the experimental work [21], which applied a High Fluctuation (HF) spectral visualization approach to emphasize dominant intensity variations in both electrolyte and nonelectrolyte solutions. As part of this enhancement, a baseline correction filter and high-pass frequency threshold were implemented to reduce noise and baseline drift, ensuring signal clarity before conversion. The acquired signal matrices are transformed into two-dimensional spectral images, enabling their use in a Convolutional Neural Network (CNN)- based classification framework. The signal-to-image transformation consists of two sequential stages: a logarithmic transformation to amplify perceptual contrast and a color mapping stage to project the signal values into RGB space using a predefined color map. This transformation was conducted using a consistent intensity scale across all data samples, avoiding dynamic range fluctuations that might bias learning.

In the first stage, each element of the raw signal matrix *D(i,j)* was transformed logarithmically to suppress high-intensity bias and enhance mid-range details, following standard practices in spectral preprocessing [5], [6], [21], [22], [25]. This process is mathematically expressed as Eq. (1) [22]:

$$S(i,j) = \log\left(D(i,j) + 1\right) \quad (1)$$

In the second stage, the resulting matrix *S(i,j)* was normalized and then mapped into the RGB domain using a continuous colormap ranging from blue to red, as implemented in the MATLAB rendering configuration. This transformation is defined as Eq. (2) [29], [35]:

$$I(i,j) = \text{ColormapRGB}\left(\frac{S(i,j)\ \ min(S)}{max(S)\ \ min(S)}\right) \quad (2)$$

This visualization was performed before the image preprocessing and color segmentation stages, aiming to maintain the dominant visual representation of each solution spectrum [24] and reinforced by similar studies that adopted 2D spectral transformation and signal fluctuation-based visualization in the multispectral image domain [20], [28]. By using consistent color-mapping parameters and fixed colormap limits, this step ensures homogeneous visual encoding across the dataset, improving generalization for CNN-based models. This converted image dataset was then utilized in the stages of image preprocessing, data augmentation, high fluctuation-based HSV segmentation, and two-class classification (H_2O and H_2O with NaOH) using CNN models (ResNet50, EfficientNetV2, and MobileNetV3).

A. Image Preprocessing

After obtaining spectral image from signal conversion, the next step is image preprocessing to ensure that all inputs are consistent, noise-free, and suitable for deep-learning processing. This step is crucial for enhancing model performance, training stability, and computational efficiency. In this study, preprocessing involves three main stages: cropping, resizing, and normalization. The first step removed irrelevant areas of the image, such as axis labels, scale bars, and background margins. This was done through cropping using fixed coordinates derived from MATLAB-based visualization, specifically along x = 40 to 58 and y = 438 to 470. Mathematically, cropping can be expressed as Eq. (3):

$$Icrop = \begin{cases} I(i,j), xmin \le i \le xmax, ymin \le j \le ymax \\ 0, other \end{cases} \quad (3)$$

where *I(I,j)* is the original image pixel at coordinate *(I,j)*, and *(xmin,xmax,ymin,ymax)* define the cropping boundaries. By focusing only on the active spectral

Manuscript received June 8, 2025; Revised August 20, 2025; Accepted September 5, 2025; date of publication September 10, 2025
Digital Object Identifier (**DOI**): https://doi.org/10.35882/jeeemi.v7i4.1016

region, non-informative pixels are excluded, allowing the model to concentrate on meaningful patterns. The cropped image was then resized to 224 × 224 pixels. This is a standard input size for convolutional neural network architectures, such as ResNet50, EfficientNetV2, and MobileNetV3 [11], [29]. The resizing operation was performed through bilinear interpolation, defined as Eq. (4):

$$I(x,y) = \sum_{m} \sum_{n} Icrop(m,n).(1 - |x - m|).(1 - |y - n| \quad (4)$$

where *(x,y)* are the target coordinates in the resized image, and *(m,n)* are the nearest pixel coordinates in the cropped image. This interpolation ensures smooth scaling while preserving spectral information. Resizing ensures consistent dimensions across training batches, simplifying the network architecture by eliminating the need for dynamic input reshaping. The final step in preprocessing is pixel normalization. Each RGB channel is scaled to a range of [0,1], reducing the influence of large pixel values and enhancing gradient flow during training. This normalization accelerates convergence and minimizes the risk of vanishing or exploding gradients [3], [33]. Mathematically, the operation is defined as Eq. (5):

$$\mathrm{Inorm(i,j,c)} = \frac{Iresize(i,j,c)}{255} \quad (5)$$

where *(i,j)* represent pixel coordinates and $c \in \{R,G,B\}$ indicates the respective color channel. This preprocessing strategy aligns with best practices in spectral image processing, as demonstrated in water leakage detection using TinyML [26], HSV-based thermal spectrum classification [20], [21], and fluid segmentation preprocessing [3], [22]. These references collectively support the importance of structured preprocessing in enhancing classification robustness across diverse spectral datasets.

B. Augmentation

In deep learning-based spectral image classification, data augmentation is a crucial technique for increasing variability within the training dataset and mitigating overfitting, particularly when the number of training samples is limited. Given the high visual similarity between the two classes (H_2O and H_2O + NaOH), augmentation serves to introduce controlled distortions that mimic possible environmental variations. This becomes essential when dealing with visually similar spectral patterns, such as distinguishing between pure H_2O and H_2O mixed with NaOH, where both exhibit subtle differences in color and intensity. By artificially enriching the dataset, augmentation enables the CNN model to generalize more effectively across unseen variations, thereby improving its robustness during inference [3], [16]. One of the fundamental augmentation strategies applied is random rotation. Images are rotated within a specified angular range, such as –30° to 30°, which helps simulate the occurrence of spectral shifts or variations due to different acquisition angles [3]. This is particularly relevant for practical implementations where image acquisition may not always be axis-aligned. This augmentation enhances the model's ability to recognize key spectral structures across varying orientations, supporting rotation-invariant learning. This approach is practical in several visual classification domains, including spectral and medical imaging [14]. In addition to rotation, horizontal and vertical flipping was employed to generate symmetrical variations of the original image. Flipping preserves the core spectral features, while expanding the diversity of directional patterns observed by the model [21]. This approach maintains the structural integrity of spectral information while enhancing generalization across mirror-transformed variants, a method that has proven beneficial in fluid pattern analysis and spectral object detection [9].

Another commonly used technique is zooming, or random scaling, aiming to simulate differences in observation distance or field of view during spectral signal acquisition and image transformation. By performing moderate zooming, this transformation ensures that the central spectral region remains visible while training the network to handle size variance and spatial scaling [16]. Such augmentations enhance model flexibility in learning size-invariant features across spectral datasets [19]. Finally, contrast and brightness adjustments were applied to simulate illumination inconsistencies that may arise from signal-to-image conversion, especially under varying experimental conditions. Modifying these visual attributes ensures that the model does not overfit to specific lighting environments and can instead capture meaningful features under diverse image conditions [14] . This step has been validated in studies involving both biomedical imaging and spectral classification, showing increased performance stability when faced with varying illumination patterns [19].

All augmentation techniques were implemented using the `ImageDataGenerator` module from the Keras library, which performs real-time image transformation during training. This implementation not only expands the dataset virtually but also stabilizes training convergence and enhances model generalization. The combination of these techniques has been proven to significantly enhance the classification performance of CNNs, especially in domains with constrained data availability, such as spectral imaging, remote sensing, and microscopic analysis [20], [26], [27], [30] .

C. Segmentation Method and Approach

Manuscript received June 8, 2025; Revised August 20, 2025; Accepted September 5, 2025; date of publication September 10, 2025
Digital Object Identifier (**DOI**): https://doi.org/10.35882/jeeemi.v7i4.1016

Image segmentation plays a crucial role in the multispectral image classification pipeline, particularly in highlighting regions with significant spectral variance. In this study, segmentation was conducted through a color space-based approach using HSV (Hue, Saturation, Value), with a focus on isolating the violet-blue spectral zone, which prior studies have identified as the most responsive to chemical mixing between H_2O and NaOH. The segmentation procedure consists of three sequential stages: (1) hue range masking in HSV space, (2) suppression of edge noise using Gaussian smoothing, and (3) bitwise masking to extract active spectral zones from the RGB image.

1. HSV-Based Spectral Segmentation

The original RGB image was first transformed into HSV color space to enable range-based masking of the hue component. The hue values in the interval [110, 170] were selected to capture spectral shifts toward violet-blue colors [2], which have been shown to correlate with changes in temperature and solute density following the addition of NaOH [9], [19]. The mask was formed by thresholding the HSV values as follows (Eq. (6)):

$$M(i,j) = \begin{cases} 1, if\ 110 \le H(i,j) \le 170, S(i,i) \ge 30, V(i,j) \ge 50 \\ 0, other \end{cases} \quad (6)$$

where *H(i,j), S(i,j), and V(i,j)* represent the hue, saturation, and value at pixel *(i,j)*, and *M(i,j*) denotes the binary mask.

2. High Fluctuation (HF) Region Emphasis

To enhance mask precision, the binary mask was refined through Gaussian blurring, which suppresses local noise and highlights smoother boundaries between active and inactive regions. This step corresponds to the High Fluctuation (HF) emphasis, as it helps preserve only the most visually dynamic areas, consistent with prior spectral fluctuation models proposed. [2], [21], [24]. The Gaussian smoothing is expressed as Eq. (7):

$$Mblur = GaussianBlur(M, K = (5,5), \sigma = 0) \quad (7)$$

where *M* denotes the binary mask generated from the segmentation stage, *K* represents the convolution kernel size (5×5 in this study), and *σ* is the Gaussian standard deviation controlling the level of smoothing, set to zero to allow the function to compute it based on kernel size. This technique was inspired. [2], [21], [24] who utilized frequency domain transformation and variance statistics to reveal hidden spectral information that was often masked by background noise.

3. Final Masking and Spectral Output

The blurred mask was then applied to the original RGB image through pixel-wise masking to extract only the active spectral components. The output segmented image is defined as Eq. (8):

$$Isegment(i,j) = I(i,j)\ x\ \frac{Mblur(i,j)}{255} \quad (8)$$

where *I(i,j)* denotes the original RGB pixel value and *Isegment(i,j)* is the resulting segmented pixel. This segmentation approach enhances classification by discarding noninformative pixels and has proven effective in diverse CNN-based applications involving tissue imaging, fluid thermodynamics, and aerial spectral analysis [3], [5], [8], [24].

D. Classification Method

This study employed an ensemble learning approach based on Convolutional Neural Networks (CNN) to classify images derived from spectrum segmentation results into two main classes: H_2O and H_2O with NaOH.

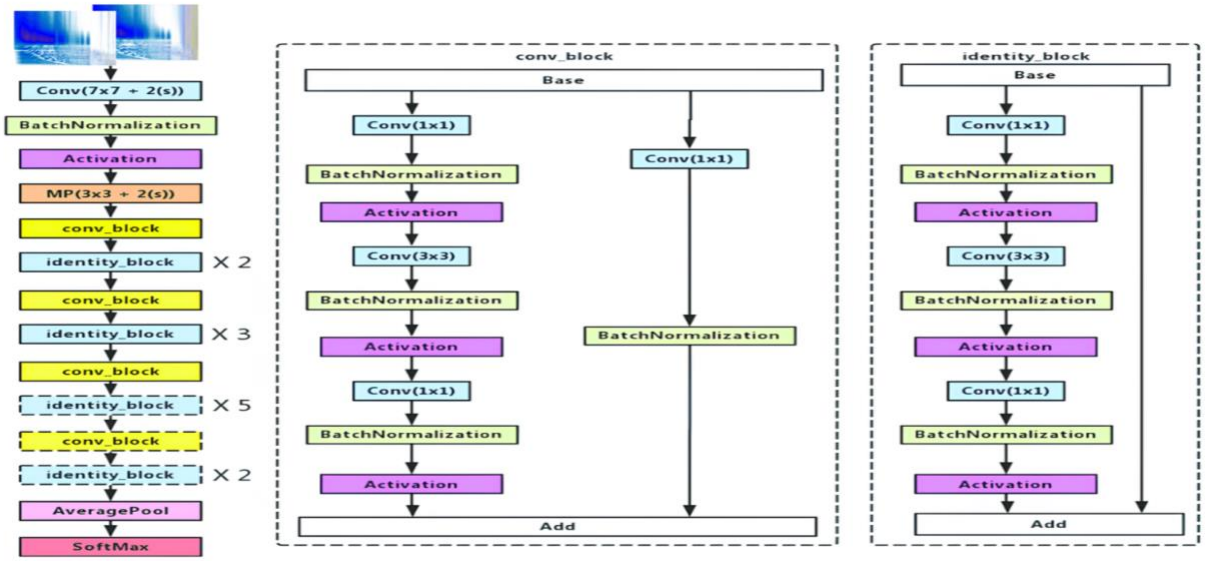

Fig. 2. Illustration architecture of Resnet50

Manuscript received June 8, 2025; Revised August 20, 2025; Accepted September 5, 2025; date of publication September 10, 2025
Digital Object Identifier (**DOI**): https://doi.org/10.35882/jeeemi.v7i4.1016

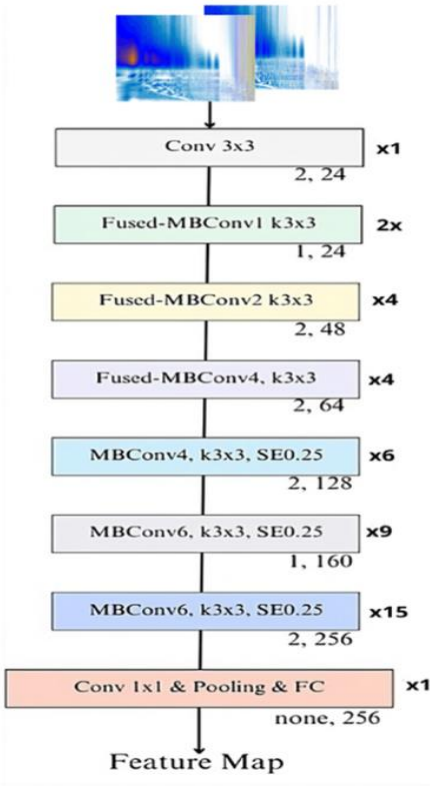

Fig. 3. Illustration architecture of EfficientNetV2

The three selected CNN architectures, ResNet50, EfficientNetV2, and MobileNetV3, were selected based on their complementary strengths in terms of feature extraction, efficiency, and generalization. Each model was trained independently using identical configurations and then combined using the soft voting ensemble method.

1. CNN Architecture Used

ResNet50. ResNet50 is a deep Convolutional Neural Network (CNN) architecture that utilizes a residual learning mechanism to prevent accuracy degradation as the network deepens. The residual block enables better gradient propagation and accelerates convergence. As illustrated in Fig. 2, the ResNet50 architecture employs stacked residual blocks that facilitate efficient feature extraction. This model has been widely used in medical and satellite image classification [2] [4] to capture subtle spectral patterns that arise due to changes in the chemical composition of the environment [25]. In this study, ResNet50 was used with pre-trained weights from ImageNet, modified at the end for two class classifications. The input image used is the result of HSV segmentation measuring 224×224 pixels. The training process reaches optimal convergence in 12 epochs. Previous studies have demonstrated that ResNet50 achieves an accuracy of over 96% in cancer classification [6] and was also utilized for spectral imaging-based chemical feature detection in the agricultural and medical fields [8].

EfficientNetV2. EfficientNetV2 is the next generation of EfficientNet, designed with a combined scaling approach that expands the network equally in depth, width, and resolution. Its main feature is the combination of MBConv and Fused MBConv blocks [9], which shortens training time while maintaining the efficiency parameters [3]. Fig. 3 illustrates the EfficientNetV2 architecture, which balances depth and width scaling, making it highly effective for medium-sized spectral datasets such as those in this study. This model is particularly suitable for medium-sized spectral data, such as those used in this study, as it requires low computing power while still producing high accuracy. In this implementation, the EfficientNetV2 variant was used with pre-trained weights from ImageNet. The model stops automatically at the 40th epoch through the Early Stopping mechanism. Recent studies have shown that EfficientNetV2 can handle nonlinear datasets such as fluid images, where dominant features are not necessarily spatial but emerge in hidden spectral transitions.

MobileNetV3. MobileNetV3 is designed for embedded systems and real-time applications, combining depth-wise separable convolutions, Squeeze and Excitation (SE) blocks, and Swish activations that are more efficient than ReLU [10]. As depicted in Fig. 4, MobileNetV3 integrates lightweight convolutional layers with SE blocks, enabling efficient learning with minimal resource usage. Despite its lightweight, this model can maintain competitive accuracy on complex data with minimal resource consumption [5], [16]. In this study, MobileNetV3 was used as a baseline lightweight classifier to verify that the segmentation and preprocessing systems used can support the performance of small models. The model shows stable convergence up to the 22nd epoch, with very competitive evaluation results. The advantages of MobileNetV3 in spectral image classification primarily lie in its inference speed and memory efficiency, making it ideal for portable multispectral camera-based real-time or edge computing implementations.

2. Strategy Ensemble

Each model was trained independently for 150 epochs with early stopping, and then the prediction results were combined using a soft voting method to obtain the final output of the ensemble. The architectures were chosen based on an evaluation of recent CNN libraries, which showed that these three models complement each other in terms of efficiency, feature extraction depth, and inference speed. The choice of hyperparameters, such as batch size (32), learning rate (0.001), and the use of the Adam optimizer, was based on preliminary experiments aimed at maximizing

Manuscript received June 8, 2025; Revised August 20, 2025; Accepted September 5, 2025; date of publication September 10, 2025
Digital Object Identifier (**DOI**): https://doi.org/10.35882/jeeemi.v7i4.1016

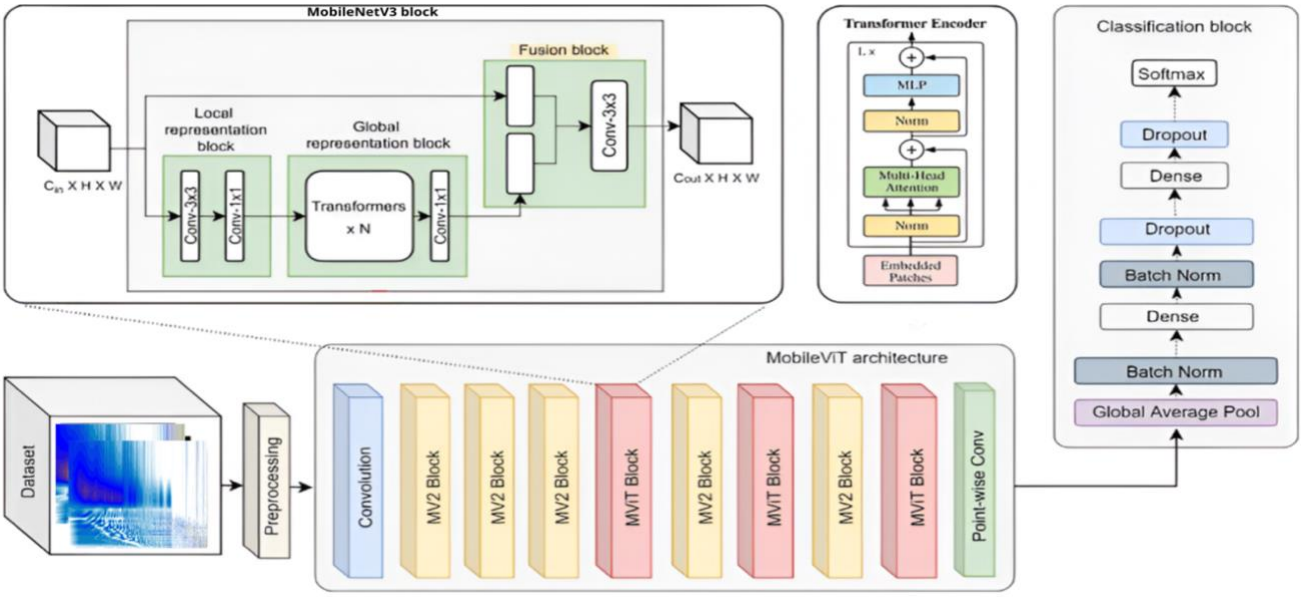

Fig. 4. Ilustration architecture of MobileNetV3

convergence speed while avoiding overfitting. Early stopping was applied to terminate training when validation loss stagnated, ensuring model generalization. No extensive grid search was performed due to computational constraints, but default configurations yielded stable results across all models.

A. Evaluation

A comprehensive performance evaluation of classification was conducted on the ResNet50, EfficientNetV2, and MobileNetV3 models using a pre-separated test dataset. To ensure the clarity of the prediction model in distinguishing between H_2O and H_2O with NaOH solutions, several key evaluation metrics were used, namely:

Accuracy the proportion of correct predictions compared to total predictions (Eq. (9)).

$$\text{Accuracy} = \frac{TP+TN}{TP+TN+FN+FP} \times 100 \quad (9)$$

Precision the model's ability to avoid false positives in each class (Eq. (10)).

$$\text{Precision} = \frac{TP}{TP+FP} \times 100 \quad (10)$$

Recall (Sensitivity) the extent to which the model successfully captures all data from each class (Eq. (11)).

$$\text{Recall} = \frac{TP}{TP+FN} \times 100 \quad (11)$$

F1 Score harmonization between precision and recall, which is useful when classes are unbalanced (Eq. (12)).

$$\text{F1 Score} = 2 \times \frac{Recall \times Precision}{Recall + Precision} \quad (12)$$

The evaluation was conducted in three stages: data training, data validation, and final data testing. The dataset was randomly split into 70% training, 15% validation, and 15% testing sets. Stratified sampling was applied to maintain balanced class distributions across all subsets, and data leakage was prevented by ensuring no overlapping images appeared in more than one set. The test results were analyzed not only in terms of numerical performance but also in terms of generalization tendencies between models. Graphical evaluation was also performed by visualizing the accuracy and loss curves against epochs, as well as the confusion matrix, which illustrates the model's ability to distinguish between very similar fluid spectra visually. This method is supported by an evaluation approach that has been widely used in the CNN and spectral classification literature [27], which emphasizes the importance of quantitative and qualitative analysis for the validation of spectral visualization-based models [17], [31].

III. Result

Classification experiments were conducted on multispectral image datasets from two environmental classes: H_2O (295 images) and H_2O with NaOH (512 images), totaling 807 images. All photos have undergone HF-based segmentation, normalization, and augmentation stages, as described in Chapter 2.

Manuscript received June 8, 2025; Revised August 20, 2025; Accepted September 5, 2025; date of publication September 10, 2025
Digital Object Identifier (**DOI**): https://doi.org/10.35882/jeeemi.v7i4.1016

Fig. 5. Epoch results using Resnet50 architecture: (a) Accuracy vs. epoch; (b) Loss vs. epoch

Fig. 6. Epoch results using EfficientNetV2 architecture: (a) Accuracy vs. epoch; (b) Loss vs. epoch

Fig. 7. Epoch results using MobileNetV3 architecture: (a) Accuracy vs. epoch; (b) Loss vs. epoch

Manuscript received June 8, 2025; Revised August 20, 2025; Accepted September 5, 2025; date of publication September 10, 2025
Digital Object Identifier (**DOI**): https://doi.org/10.35882/jeeemi.v7i4.1016

The data were divided into three main subsets: 64% for training, 16% validation, and 20% testing. Three CNN models, ResNet50, EfficientNetV2, and MobileNetV3, were trained independently using the same parameters: a maximum of 150 epochs, a batch size of 32, and optimization with Adam (learning rate of 0.0001). Evaluation was performed using accuracy, precision, recall, f1 score, and loss metrics. Additional visualizations, including accuracy and loss curves, as well as confusion matrices, were used to assess the training process and final classification performance.

A. Image Classification Performance

The HF segmentation images show significant spectral patterns in distinguishing H_2O and its mixture with NaOH, although the differences are not visible to the naked eye. A CNN model was drilled to automatically recognize these patterns based on color and spectral intensity information. The training data distribution included 515 images (188 H_2O and 327 H_2O with NaOH), while the validation included 128 images (47 H_2O and 81 H_2O with NaOH). All models showed stable convergence.

B. Training Results and Dataset Validation

The training and validation processes in this study were conducted separately for three CNN architectures: ResNet50, EfficientNetV2, and MobileNetV3, using multispectral segmentation images from two classes: H_2O and H_2O with NaOH. The evaluation of training performance is illustrated through the accuracy and loss curves against the number of epochs, as shown in Fig. 5, Fig. 6, and Fig. 7. Each graph consists of two curves that indicate how well the model performs during the learning process. The blue curve represents the evaluation results on the training dataset, illustrating how the model adapts to the patterns observed during supervised learning. Meanwhile, the red curve depicts the model's performance on the validation dataset, which is critical in assessing generalization capability to unseen data.

The behavior of these two curves, whether they converge, diverge, or remain stable, offers insight into how effectively the model learns without overfitting or underfitting. The accuracy curve represents the extent to which the model accurately recognizes patterns in the data, while the loss curve indicates the level of model prediction error. The patterns of both curves were evaluated to understand the extent to which the model experiences convergence and to detect potential overfitting or learning synchronization. This practice is a common approach used to stabilize the training process and generalize the model to data not seen during training [12]. In Fig. 5, the ResNet50 architecture achieves rapid convergence within 12 epochs. The training accuracy curve increases dramatically from around 68% to over 95%, and the validation accuracy reaches over 90% since the 4th epoch and remains stable. The loss curve exhibits a sharp decrease from 1.7 to below 0.2 during training, and the validation loss remains low at approximately 0.3. This stability indicates that the model successfully recognizes essential patterns in the data without overfitting.

Fig. 6 shows the results of training EfficientNetV2 for 40 epochs. Validation accuracy increases very rapidly in the first five epochs, even surpassing training accuracy. Over time, accuracy catches up with training and reaches around 89%. Training loss drops from 2.5 to below 0.4, while validation loss remains stable below 0.3. Such behavior generally indicates a high degree of regularization and good generalization ability, where the model not only adapts to the training data but also maintains high accuracy on new data [12]. Meanwhile, Fig. 7 shows the performance of MobileNetV3 up to the 22nd epoch. Despite being a lightweight architecture, the model achieves validation accuracy above 90% quickly and stably. The training accuracy increases from 53% to approximately 88%, indicating a notable progressive improvement. The training loss drops drastically from over 5 to around 0.4, and the validation loss remains low without significant attrition, suggesting that even lightweight models can be drilled effectively if supported by proper preprocessing and segmentation.

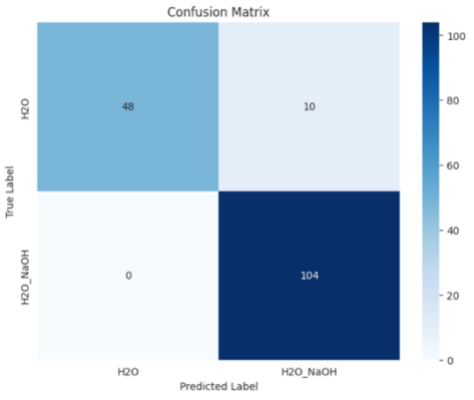

Fig. 8. Testing Result Using Resnet50

Overall, all three CNN architectures exhibit clear signs of training stability and convergence across both training and validation datasets. ResNet50 achieves rapid convergence and low validation loss, with no significant divergence, suggesting minimal risk of overfitting. EfficientNetV2 displays regularized behavior, as seen by the initial higher validation accuracy than training, indicating strong generalization capability. MobileNetV3, despite being a lightweight model, also demonstrates stable improvement without overfitting signs, although with a slower initial learning

Manuscript received June 8, 2025; Revised August 20, 2025; Accepted September 5, 2025; date of publication September 10, 2025
Digital Object Identifier (**DOI**): https://doi.org/10.35882/jeeemi.v7i4.1016

rate. The behavior of the accuracy and loss curves in Fig. 5, Fig. 6, and Fig. 7 confirms that each model successfully learns the spectral distinctions between H_2O and H_2O with NaOH, with no evident instability, noise sensitivity, or training collapse, fulfilling the requirements for robust classification.

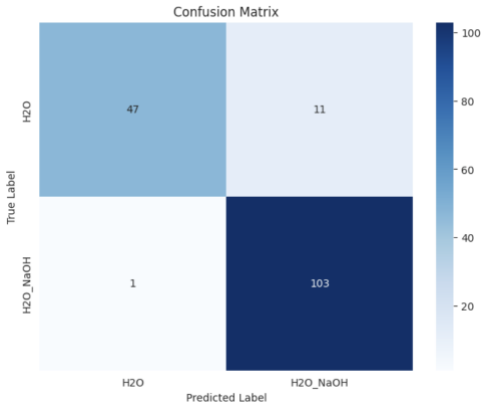

Fig. 9. Testing results using EfficientNetV2

C. Validation Of Testing Results on The Dataset

The evaluation model in this study was conducted using a multispectral image dataset from the experimental results consisting of a total of 807 images, divided into 295 images for the H_2O class and 512 images for the H_2O with NaOH class. All of these images have gone through a color segmentation and augmentation process before being used in training, validation, and testing. The dataset is divided into three main parts, namely training data, validation data, and testing data. A total of 64% of the data was used for training, 16% for validation, and 20% was used as the final test data. In these proportions, the test data consists of 162 images, namely 58 images from the H_2O class and 104 images from the H_2O with NaOH class. The test results are displayed through a confusion matrix for each model, aiming to visually and numerically describe the classification performance of the two main classes. In ResNet50, as shown in Fig. 8, the model successfully classified all 104 H_2O with NaOH images correctly but misclassified 10 out of 58 H_22O images, which were mistaken for mixed solutions. This indicates that ResNet50 exhibits excellent detection capability for alkaline environments; however, it still tends to over-detect spectra resembling H_2O with NaOH in some pure H_2O images.

Meanwhile, EfficientNetV2, as shown in Fig. 9, successfully classifies 47 out of 58 H_2O images correctly and 103 out of 104 H_2O with NaOH images correctly. This model shows a good classification balance between classes, with errors that are almost uniform but still small. The efficiency of this architecture is reflected in its ability to maintain generalization to very similar spectral distributions between the two classes.

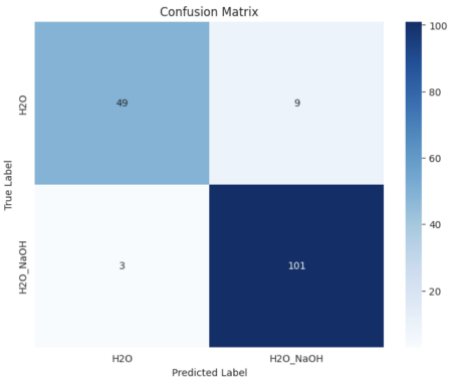

Fig. 10. The testing results using MobileNetV3

On MobileNetV3, as shown in Fig. 10, the test results indicate that this lightweight model can provide competitive results. A total of 49 H_2O images were correctly classified, and 101 out of 104 H_2O with NaOH images were successfully recognized. The classification error is slightly higher than that of the other two models but remains within acceptable limits, considering the computational efficiency offered by this architecture.

Table 1. The comparison of the accuracy of achievements of the three architectures

CNN's Architecture	Accuracy	Precision	Recall	F1 Score
Resnet50	93.83%	94.36%	93.82%	93.67%
EfficientNetv2	92.52%	93.05%	92.59%	92.41%
MobileNetV3	92.59%	92.68%	92.59%	92.49%

This section discusses the performance comparison and practical implications of the classification models based on the results presented earlier. Overall, all architectures demonstrate strong test performance on complex multispectral image datasets. ResNet50 demonstrates strength in high precision for base solutions; EfficientNetV2 provides the most balanced classification, while MobileNetV3 shows that architectural efficiency does not necessarily mean a compromise on accuracy, making it an ideal candidate for real-time applications on lightweight devices.

IV. Discussion

The classification results demonstrate that ResNet50, EfficientNetV2, and MobileNetV3 are capable of distinguishing subtle spectral variations between H_2O and H_2O with NaOH after preprocessing with HF segmentation. As summarized in Table 1, ResNet50 achieved the highest accuracy of 93.83% and F1-score of 93.67%, followed closely by EfficientNetV2 and MobileNetV3, both of which maintained accuracy above 92%. The high accuracy obtained, particularly by

Manuscript received June 8, 2025; Revised August 20, 2025; Accepted September 5, 2025; date of publication September 10, 2025
Digital Object Identifier (**DOI**): https://doi.org/10.35882/jeeemi.v7i4.1016

ResNet50, indicates that residual learning plays a vital role in extracting deep spectral features. EfficientNetV2, on the other hand, shows that compound scaling of depth and width can provide robust regularization, while MobileNetV3 proves that lightweight models remain competitive when supported by proper preprocessing. These results collectively suggest that preprocessing through HF segmentation is the decisive factor that allows CNN architectures to effectively capture discriminative spectral features that are not readily perceivable by human vision.

Our findings are consistent with recent research on hyperspectral and multispectral classification tasks. For example, Zhang et al. [25] reported that ResNet-based models outperformed traditional CNNs in hyperspectral vegetation classification, particularly in terms of recall, aligning with our observation of ResNet50's sensitivity. Similarly, Liang et al. [16] demonstrated that lightweight architectures such as MobileNetV3 could achieve competitive accuracy for image classification in resource-limited devices, supporting our findings on MobileNetV3's efficiency. In addition, LONG Jianing et al.[8] emphasized the role of preprocessing and augmentation in boosting EfficientNet performance, which parallels the strong generalization of EfficientNetV2 in our study. These comparisons indicate that our research fits within the broader trend of leveraging both advanced CNNs and preprocessing strategies to improve spectral classification.

Despite promising results, some limitations must be acknowledged. First, the dataset used in this study is limited to binary classification (H_2O and H_2O with NaOH), which constrains the generalizability of the findings to more complex chemical mixtures. Second, the spectral images were generated from laboratory-controlled experiments, and the robustness of the models under real-world imaging conditions (e.g., noise, lighting variability, impurities) remains untested. Third, hyperparameter tuning was relatively limited, and further exploration of alternative optimizers or regularization strategies could potentially enhance performance. These limitations open avenues for additional research to extend and validate the applicability of the proposed approach.

The implications of this work are twofold. From a scientific standpoint, the integration of HF segmentation with CNN ensembles provides a reproducible framework for distinguishing subtle spectral differences in chemical solutions. This can inform future studies in analytical chemistry and spectral imaging by highlighting the importance of preprocessing in feature enhancement. From a practical perspective, the demonstration that lightweight models such as MobileNetV3 can achieve high accuracy suggests strong potential for real-time deployment in portable devices and industrial monitoring systems. Moreover, by aligning with the No-Free-Lunch Theorem [15], our study underlines the importance of selecting models based on application-specific needs rather than seeking a universally superior architecture.

V. Conclusion

This study aimed to develop a multispectral image classification system based on High Fluctuation (HF) segmentation and an ensemble of three CNN architectures, ResNet50, EfficientNetV2, and MobileNetV3, to distinguish between pure water (H_2O) and H_2O mixed with NaOH, which exhibit very subtle spectral differences visually. The main findings show that the proposed approach achieves high classification performance. ResNet50 recorded the highest accuracy of 93.83%, with a precision of 94.36%, a recall of 93.82%, and an F1-score of 93.67%. EfficientNetV2 achieved an accuracy of 92.52% with strong convergence and lower validation loss, while MobileNetV3 maintained a competitive accuracy of 92.59% with superior computational efficiency suitable for lightweight applications. An additional finding is that HF-based spectral segmentation in the HSV color space significantly enhances model stability and convergence, confirming its importance as a preprocessing step for distinguishing chemical solutions with overlapping spectral features. Future work can be directed at expanding the classification to include more chemical solution classes, investigating advanced architectures such as attention-based networks and Vision Transformers, and deploying the system in portable or edge-computing devices for real-time industrial applications.

Acknowledgment

The authors would like to thank LPPM of Universitas Syiah Kuala for its continuous support and for providing the research facilities that enabled the successful completion of this study.

Funding

This research was supported by the H Index Research Grant from Universitas Syiah Kuala under contract number: 532/UN11/SPK/PNBP/2019.

Author Contribution

Melinda Melinda, designed the central concept and idea of the study, was responsible for funding acquisition, conducted the investigation and data collection, and wrote the initial draft of the manuscript. Yunidar Yunidar was accountable for the development and design of the methodology used in this study. Zulhelmi Zulhelmi supervised the research process and validated the results. Lailatul Qadri Zakaria carried out formal

Manuscript received June 8, 2025; Revised August 20, 2025; Accepted September 5, 2025; date of publication September 10, 2025
Digital Object Identifier (**DOI**): https://doi.org/10.35882/jeeemi.v7i4.1016

statistical analysis and data interpretation. Arya Suyanda managed the data curation and created data visualizations in the form of tables and figures. W.K. Wong performed a critical review and final editing of the manuscript. All authors have read, reviewed, and approved the final version of the manuscript for publication.

Declarations

Consent for Publication Participants.

Consent for publication was given by all participants

Competing Interests

The authors declare no competing interests.

References

[1] Egesa, AO, Davidson, M.T., Pérez, H.E., & Begcy, K. (2024). Biochemical And Physical Screening Using Optical Oxygen Sensing And Multispectral Imaging In Sea Oats Seeds. Agriculture,14(6),875.Https://Doi.Org/10.3390/Agriculture14060875

[2] Yücel, N., Yildirim, M., & Aslan, S. (2023). Performances Of Pre Trained Models In Classification Of Body Cavity Fluid Cytology Images.Http://As Proceeding.Com/:Konya,Turkeyhttps://Www.Icaens.Com/

[3] Cai, W., Li, M., Jin, G., Liu, Q., & Lu, C. (2024). Comparison Of Residual Network And Other Classical Models For Classification Of Interlayer Distresses In Pavement. Applied Sciences (Switzerland), 14(15).Https://Doi.Org/10.3390/App14156568

[4] Kim, R., & Kim, A. (2024). Analysis Of Modern Computer Vision Models For Blood Cell Classification. Https://Doi.Org/10.48550/Arxiv.2407.00759

[5] Riccardi Advisor, M., Marcon Co Advisor, M., & Ugo Leonzio, D. (2022). Multispectral Imaging For Solvent Classification Using NIR & Visible Spectra Laurea Magistrale In Mathematical Engineering Ingegneria Matematica. Https://Www.Politesi.Polimi.It/Retrieve/B07bbaffB44b 425d B21a 78ea9c8c86e9/Executive_Riccardi_Sensor_VIS_IR.Pdf

[6] Melinda, S. T. A., Sudiana, D., Gunawan, D., & Iqbal, M. (2016). Implementation Of Segmentation Scheme Based On Wavelet Transform In Multi Spectral Fluctuation Patterns. Https://Jtec.Utem.Edu.My/Jtec/Article/View/1434

[7] Melinda, M., Tamsir, A. S., Afifah, S., & Gunawan, D. (2018). Impedance Influence Analysis On Multi Spectral Capacitive Sensor. 2018 International Conference On Electrical Engineering And Informatics (Iceltics)(44501), 19 24. Https://Doi.Org/10.1109/ICELTICS.2018.8548794

[8] LONG Jianing, Z. Z. L. X. L. Y. R. Z. Y. J. Z. M. F. P. H. Z. H. C. W. X. (2023). Wheat Lodging Types Detection Based On UAV Image Using Improved Efficientnetv2. Https://Doi.Org/10.12133/J.Smartag.SA202308010

[9] Saeed, A., Shaukat, S., Shehzad, K., Ahmad, I., Eshmawi, A.A., Amin, A.H., & Tag Eldin, E. (2022). A Deep Learning Based Approach For The Diagnosis Of Acute Lymphoblastic Leukemia. Electronics (Switzerland), 11(19).Https://Doi.Org/10.3390/Electronics11193168

[10] Bukhari, MT (2024). Efficacy Of Lightweight Vision Transformers In The Diagnosis Of Pneumonia.Https://Doi.Org/10.1101/2024.10.24.24316057

[11] Badruzzaman, A., & Arymurthy, A. M. (2024). Sharealike 4.0 International License (CC BY SA 4.0). How To Cite: Ahmad Badruzzaman And Aniati Murni Arymurthy, A Comparative Study Of Convolutional Neural Network In Detecting Blast Cells For Diagnose A Comparative Study Of Convolutional Neural Network In Detecting Blast Cells For Diagnose Acute Myeloid Leukemia. Journal Of Electronics, Electromedical Engineering, And Medical Informatics, 6(1), 84 91.Https://Doi.Org/10.35882/Jeemi.V6i1.354

[12] Chirikhina, E., Chirikhin, A., Dewsbury Ennis, S., Bianconi, F., & Xiao, P. (2021). Skin Characterization By Using Contact Capacitive Imaging And High Resolution Ultrasound Imaging With Machine Learning Algorithms. Applied Sciences (Switzerland), 11(18).Https://Doi.Org/10.3390/App11188714

[13] Arefi, F., Mansourian, A. M., & Kasaei, S. (2024). Deep Spectral Improvement For Unsupervised Image Instance Segmentation. PLOS ONE, 19(10), E0307432. Https://Doi.Org/10.1371/Journal.Pone.0307432

[14] Yarahmadi, P., Ahmadpour, E., Moradi, P., & Samadzadehaghdam, N. (2025). Automatic Classification Of Giardia Infection From Stool Microscopic Images Using Deep Neural Networks. Bioimpacts, 15.Https://Doi.Org/10.34172/Bi.30272

[15] Rashki, M., & Faes, M. G. R. (2023). No Free Lunch Theorems For Reliability Analysis. ASCE ASME Journal Of Risk And Uncertainty In Engineering Systems, Part A: Civil Engineering,

Manuscript received June 8, 2025; Revised August 20, 2025; Accepted September 5, 2025; date of publication September 10, 2025
Digital Object Identifier (**DOI**): https://doi.org/10.35882/jeeemi.v7i4.1016

9(3). Https://Doi.Org/10.1061/AJRUA6.RUENG 1015

[16] Liang, X., Liang, J., Yin, T., & Tang, X. (2023). A Lightweight Method For Facial Expression Recognition Based On Improved Mobilenetv3. IET Image Processing, 17(8), 2375 2384.Https://Doi.Org/10.1049/Ipr2.12798

[17] Lu, L., Qi, W., Bing, W., Shichao, F., Li, L., & Qingjie, L. (2021). Water Body Extraction From High Resolution Remote Sensing Images Based On Scaling Efficientnets. Journal Of Physics: Conference Series, 1894(1).Https://Doi.Org/10.1088/1742 6596/1894/1/012100

[18] Vali, A., Comai, S., & Matteucci, M. (2020). Deep Learning For Land Use And Land Cover Classification Based On Hyperspectral And Multispectral Earth Observation Data: A Review. In Remote Sensing (Vol. 12, Issue 15). MDPI AG.Https://Doi.Org/10.3390/RS12152495

[19] Wang, M., Liu, W., Gu, X., Cui, F., Ding, J., Zhu, Y., Bian, J., Chen, Y., & Zhou, J. (2024). Few Shot Learning To Identify Atypical Endometrial Hyperplasia And Endometrial Cancer Based On Transvaginal Ultrasonic Images. Heliyon, 10(16).Https://Doi.Org/10.1016/J.Heliyon.2024. E36426

[20] Junidar, J., Melinda, M., Diannuari, DD, Acula, DD, & Zainal, Z. (2025). FACE AUTISTIC CLASSIFICATION BASED ON THERMAL USING IMAGE ENSEMBLE LEARNING OF VGG 19, RESNET50V2, AND EFFICIENTNET. Radioelectronics And Computer Systems, 2025(1(113)), 153 164.Https://Doi.Org/10.32620/Reks.2025.1.11

[21] Melinda, M., Tanjung, A., Tamsir, A. S., Basari, B., & Gunawan, D. (2017). Grouped Data Analysis Of H_2O And H_2O Mixed With Naoh On Multi Spectral High Fluctuation Pattern. 2017 International Conference On Electrical Engineering And Informatics (Iceltics), 184 188. Https://Doi.Org/10.1109/ICELTICS.2017.82532 66

[22] Melinda, Tamsir, A. S., Basari, & Gunawan, D. (2016). Analysis Of Consistence Level Using New Method Of Statistical Transformation Approach In Multi Spectral Fluctuation Pattern. 2016 6th IEEE International Conference On Control System, Computing And Engineering (ICCSCE), 251 255. Https://Doi.Org/10.1109/ICCSCE.2016.7893580

[23] Melinda, M., Yunidar, Y., Noufal, Z., Prasetyo, AB, & Irhamsyah, M. (2022). A Novel Subtraction Method For Signal Fluctuation. 2022 5th International Seminar On Research Of Information Technology And Intelligent Systems, ISRITI 2022, 700 705.Https://Doi.Org/10.1109/ISRITI56927.2022. 10052936

[24] Melinda, M., Tamsir, A. S., Basari, B., & Gunawan, D. (2017). Performance Of Consistency Parameters Analysis Using Fourier And Wavelet Transform On Multi Spectral Fluctuation Signal. 2017 International Conference On Electrical Engineering And Informatics (Iceltics), 7 11. Https://Doi.Org/10.1109/ICELTICS.2017.82532 48

[25] Zhang, S., Yuan, Y., Wang, Z., Wei, S., Zhang, X., Zhang, T., Song, X., Zou, Y., Wang, J., Chen, F., & Li, J. (2025). A Novel Deep Learning Model For Spectral Analysis: Lightweight Resnet CNN With Adaptive Feature Compression For Oil Spill Type Identification. Spectrochimica Acta Part A: Molecular And Biomolecular Spectroscopy, 329, 125626. Https://Doi.Org/10.1016/J.Saa.2024.125626

[26] Jackson, A. (2021). Smart Buildings: Water Leakage Detection Using Tinyml Edificios Inteligentes: Detección De Fugas De Agua Utilizando Tinyml (Vol. 2, Issue 1). Https://Orcid.Org/0009 0000 3207 7238www.Infotechjournal.Org

[27] Dong, S., Feng, W., Quan, Y., Dauphin, G., Gao, L., & Xing, M. (2022). Deep Ensemble CNN Method Based On Sample Expansion For Hyperspectral Image Classification. IEEE Transactions On Geoscience And Remote Sensing, 60. Https://Doi.Org/10.1109/TGRS.2022.3183189A nalysis. Complexity, 2020.Https://Doi.Org/10.1155/2020/8361989

[28] Li, J., He, Z., Li, D., & Zheng, A. (2022). Research On Water Seepage Detection Technology For Tunnel Asphalt Pavement Based On Deep Learning And Digital Image Processing. Scientific Reports, 12(1).Https://Doi.Org/10.1038/S41598 022 15828 W

[29] Gupta, S., D., U., & Hebbar, R. (2022). *Analysis and application of multispectral data for water segmentation using machine learning*. http://arxiv.org/abs/2212.08749

[30] Kirby, K., Ferguson, S., Rennie, C. D., Cousineau, J., & Nistor, I. (2024). Identification of the best method for detecting surface water in Sentinel-2 multispectral satellite imagery. *Remote Sensing Applications: Society and Environment*, *36*. https://doi.org/10.1016/j.rsase.2024.101367

Manuscript received June 8, 2025; Revised August 20, 2025; Accepted September 5, 2025; date of publication September 10, 2025
Digital Object Identifier (**DOI**): https://doi.org/10.35882/jeeemi.v7i4.1016

[31] Alhichri, H. (2023). RS-DeepSuperLearner: fusion of CNN ensemble for remote sensing scene classification. *Annals of GIS*, *29*(1), 121–142. https://doi.org/10.1080/19475683.2023.2165544

[32] Anand, V., Oinam, B., & Wieprecht, S. (2024). Machine learning approach for water quality predictions based on multispectral satellite imageries. *Ecological Informatics*, *84*. https://doi.org/10.1016/j.ecoinf.2024.102868

[33] Yao, W., Lian, C., & Bruzzone, L. (2022). A CNN Ensemble Based on a Spectral Feature Refining Module for Hyperspectral Image Classification. *Remote Sensing*, *14*(19). https://doi.org/10.3390/rs14194982

[34] Müller, D., Soto-Rey, I., & Kramer, F. (n.d.). *An Analysis on Ensemble Learning optimized Medical Image Classification with Deep Convolutional Neural Networks*. https://doi.org/10.48550/arXiv.2201.11440

[35] Souza, F. E. S. de, & Rodrigues, J. I. de J. (2023). Evaluation of Machine Learning Algorithms in the Classification of Multispectral Images from the Sentinel-2A/2B Orbital Sensor for Mapping the Environmental Dynamics of Ria Formosa (Algarve, Portugal). *ISPRS International Journal of Geo-Information*, *12*(9). https://doi.org/10.3390/ijgi12090361

Author Biography

Melinda was born in Bireuen, Aceh, on June 10, 1979. She received a B. Eng degree from the Department of Electrical and Computer Engineering, Faculty of Engineering, Universitas Syiah Kuala, Banda Aceh in 2002. She completed her master degree at the Faculty of Electrical Department, University of Southampton, United Kingdom, with a concentration in field study of Radio Frequency Communication Systems in 2009. She has completed her Doctoral degree at the Department of Electrical Engineering, Engineering Faculty of Universitas Indonesia in February 2018. She has been with the Department of Electrical Engineering, Faculty of Engineering, Universitas Syiah Kuala since 2002. She is also a member of IEEE. Her research interests include multimedia signal processing and fluctuation processing. She can be contacted at email: melinda@usk.ac.id.

Yunidar was born in Banda Aceh, Aceh, on June 29th, 1974. She has been a lecturer at the Faculty of Engineering, Department of Electrical and Computer Engineering, Universitas Syiah Kuala, since March 2000. After completing her undergraduate education in Physics at Universitas Syiah Kuala, Aceh Indonesia, in 1997, she then obtained a master of engineering (MT) degree in Optoelectrotechnics and Laser Applications from the University of Indonesia, Jakarta Indonesia, in 2000. After which she has taken a doctoral degree program in electrical and computer engineering at Syiah Kuala University and graduated in 2025. She is also a member of IEEE. Her research interests include the implementation of biomedical engineering and sensors used in biomedical applications, including multimedia. She can be contacted at email: yunidar@usk.ac.id.

Zulhelmi, was born in Sigli, Aceh, on July 2nd, 1979. He received the B.Eng. degree from Universitas Syiah Kuala, Banda Aceh, Indonesia in 2003, and the M.Sc. degrees in electrical engineering from King Saud University (KSU), Riyadh Saudi Arabia in 2013. He has been a Lecturer at Electrical and Computer Engineering Department, Universitas Syiah Kuala since 2003. Now, he is completing PhD Program at Doctoral Programs of Engineering, Universitas Syiah Kuala. His research interests include electronic design, FPGAs architecture design and implementation, Microcontroller based on Internet of Things, biomedical electronics, machine learning and deep learning. You can reach him via email at zulhelmi@usk.ac.id.

Arya Suyanda was born on March 27th, 2003 in Banda Aceh. He is a student of Electrical and Computer Engineering Department, Universitas Syiah Kuala. His undergraduate studies focused on multimedia technology, and his research explored H_2O and H_2O with NaOH. He actively participates in class and continues to develop his knowledge in his field. Enrolled in the class of 2022, he is committed to expanding his expertise and gaining practical experience. His academic journey reflects his dedication to theoretical and applied learning, which prepares him to contribute to the advancement of technology in his field. He can be reached at arya.su@mhs.usk.ac.id.

Manuscript received June 8, 2025; Revised August 20, 2025; Accepted September 5, 2025; date of publication September 10, 2025
Digital Object Identifier (**DOI**): https://doi.org/10.35882/jeeemi.v7i4.1016

Dr. Lailatul Qadri Zakaria earned her Ph.D. from the University of Southampton, U.K. She is currently a Senior Lecturer at the Centre of Artificial Intelligence (CAIT), Faculty of Information Science and Technology (FTSM), Universiti Kebangsaan Malaysia (UKM). She is also a member of the Asian Language Processing (ASLAN) research group. Her research interests include natural language processing (NLP), computational linguistics, and semantic web technologies. She has contributed to various studies on text analysis and machine learning for NLP. With extensive academic experience, she actively participates in scientific publications, research collaborations, and mentoring students in the field of artificial intelligence and language technology. She can be contacted at lailatul.qadri@ukm.edu.my

W.K. Wong is a highly experienced professional engineer (P.Eng) with a strong background in the telecommunications and building services industries prior to involvement in academia. He is currently the Director of an M&E consultancy firm and serves as an Associate Professor in the Department of Electrical and Computer Engineering at Curtin University Malaysia. Dr. Wong received his PhD and Master's degrees from Universiti Malaysia Sabah in 2008 and 2016, respectively. He is a registered member of the Board of Engineers Malaysia and member of IEEE. At Curtin Malaysia, he leads the IoT Research Group, where his research focuses on biometrics, bioinformatics, sensor technology, applied machine learning, and applied optimization. He is currently assc. Prof at Curtin University Malaysia, Dept of electrical and computer engineering. he has published over 100 academic articles and actively contributes to the research community as a reviewer and editor for numerous reputable journals.

Manuscript received June 8, 2025; Revised August 20, 2025; Accepted September 5, 2025; date of publication September 10, 2025
Digital Object Identifier (**DOI**): https://doi.org/10.35882/jeeemi.v7i4.1016